

# Simulation of light scattering by biconcave Cassini ovals using the nullfield method with discrete sources

Jens Hellmers<sup>1</sup>, Elena Eremina<sup>1</sup> and Thomas Wriedt<sup>2</sup>

<sup>1</sup> Universität Bremen, FB 4, Badgasteiner Straße 3, 28359 Bremen, Germany

<sup>2</sup> Institut für Werkstofftechnik, Badgasteiner Straße 3, 28359 Bremen, Germany

E-mail: [hellmers@iwt.uni-bremen.de](mailto:hellmers@iwt.uni-bremen.de)

Received 10 June 2005, accepted for publication 18 October 2005

Published 2 December 2005

Online at [stacks.iop.org/JOptA/8/1](http://stacks.iop.org/JOptA/8/1)

## Abstract

In this paper the nullfield method with discrete sources (NFM-DS) is applied to analysis of light scattering by biconcave Cassini-like particles, which can be described as oblate discspheres with central concavities on their top and bottom. As far as we know this is a first attempt to apply a modification of the  $T$ -matrix method to model such a nonconvex object. The numerical results for different particles under different incident angles obtained by the NFM-DS are presented in the last section of the paper. For result verification the discrete source method (DSM) has been chosen. The comparison of results obtained by using both methods shows very good agreement.

**Keywords:** nullfield method, discrete sources method,  $T$ -matrix, concavities

(Some figures in this article are in colour only in the electronic version)

## 1. Introduction

For the simulation of light scattering by small particles there are a great variety of methods which have been developed over the years. An overview on these methods has been published by Wriedt [1] and Kahnert [2]. Every method has its advantages and disadvantages. A good example for this is the  $T$ -matrix method [3], also known as the nullfield method (NFM) or extended boundary condition method (EBCM), which has become quite a popular method over the years. On one side it offers big advantages as all information about the scattering characteristics of the particle can be stored into one matrix. This allows further scattering computations with low computational efforts. On the other side the conventional  $T$ -matrix method is known to have problems with particle shapes of large aspect ratios or size parameters [4]. This hinders applications of the method to compute light scattering by more realistically shaped particles. Because of this a number of modifications have been suggested to cope with this limitation, so it becomes possible to also calculate light scattering by extremely nonspherical particle shapes.

In this paper we will show that by using the nullfield method with discrete sources (NFM-DS) [5] it now even

becomes possible to calculate light scattering by particles having concavities, which has so far been considered hardly possible [6–11].

We present results for oblate discspheres with central concavities on their top and bottom sides. To describe these kinds of particles we use two-dimensional Cassini ovals that are rotated around their vertical axis. This kind of presentation can be used, for example, to approximate the shape of the human red blood cell [12–14]. As this class of objects can be described by just three parameters and can be implemented very easily into computer algorithms—in Cartesian as well as in polar coordinates—Cassini ovals are very suitable for our purpose.

To check these light scattering results we compare them with results we get from the DSM [5] which has recently been extended to model light scattering by oblate and concave objects [15]. While the NFM-DS is a modification of the nullfield method using discrete sources for field expansion, the DSM is a variant of the generalized multipole techniques (GMT) [16] using a generalized point matching scheme. A fully detailed description can be found in the book by Doicu *et al* [5].

The DSM proved itself as a reliable and especially fast method. Wriedt *et al* [17] recently compared it to the dipole–

dipole approximation (DDA), the multipole–multipole method (MMP) and the finite integration technique (FIT) for a review of different scattering methods calculating light scattering by the human red blood cell. Because of its high computational speed the DSM is a good benchmark for comparisons.

We will start with a short description of the theory of the NFM-DS. This is followed by an overview of the DSM theory as it serves as reference for the NFM-DS results. Next we will give an introduction to Cassini ovals which are the base for describing the particle shape before we present the light scattering simulation results for different particle shapes. Finally we give a summary and conclusions.

## 2. Nullfield method with discrete sources

The  $T$ -matrix method, which was developed by Waterman [3, 18], is also known as the nullfield method (NFM) or the extended boundary condition method (EBCM). It has established itself as a very popular method for calculating light scattering by particles as it enables us to obtain all information about the scattering characteristics of the particle and to store it in one matrix. So further scattering computation, e.g. orientation averaging, can be done with low computational efforts. Unfortunately, for particles with extremely nonspherical shapes, such as fibre-like long cylinders or coin-like flat cylinders, the standard NFM has problems with convergence [4]. To cope with this limitation a number of modifications to this method have been suggested, which include improved numerical methods [19], formal modifications of the single spherical coordinate-based NFM [20], different choices of basis functions [21], and the application of spheroidal coordinate formalism [22]. In this paper we use an advanced form of the NFM: the nullfield method with discrete sources (NFM-DS) as suggested by Doicu and Wriedt [5, 23, 24]. With this method it is possible to calculate light scattering by fibre-like particles [25] as well as coin-like oblate discspheres [26].

Concavities so far have been considered hardly solvable by the NFM [6–11]. There are investigations by Mugnai and Wiscombe [27] for Chebyshev particles, which can be described as deformed spheres, partly showing concavities. Comparing simulations for this kind of particles has been done by Mishchenko *et al* [28] and recently by Wauer *et al* [29].

In this paper we will show that the extension of the conventional  $T$ -matrix method using discrete sources in a complex plane is capable of calculating light scattering by oblate discspheres with concavities.

For the theory we start with a three-dimensional space  $\Omega$  consisting of the union of a closed surface  $S$  with interior  $\Omega_i$  and exterior  $\Omega_s$ .  $O$  within  $\Omega_i$  is the origin of a Cartesian coordinate system  $O_{xyz}$ . An arbitrary point in  $\Omega$  is denoted by the position vector  $r$ , while an arbitrary point on  $S$  is given by  $r'$ .  $k_t$  is the wavenumber of the region  $\Omega_t$ , where  $k_t = k\sqrt{\epsilon_t\mu_t}$ ,  $t = s, i$  and  $k = \omega/c$ . The mathematical formulation of the scattering problem consists of the Maxwell's equations

$$\nabla \times \mathbf{E}_t = jk\mu_t \mathbf{H}_t, \quad \nabla \times \mathbf{H}_t = -jk\epsilon_t \mathbf{E}_t$$

in  $\Omega_t$  ( $t = s, i$ ), the boundary conditions on the particle surface

$$\mathbf{n} \times (\mathbf{E}_0 + \mathbf{E}_s - \mathbf{E}_i) = 0, \quad \mathbf{n} \times (\mathbf{H}_0 + \mathbf{H}_s - \mathbf{H}_i) = 0$$

on  $S$  and the Silver–Müller radiation condition for  $(\mathbf{E}_s, \mathbf{H}_s)$  uniformly over all possible radial directions. Then the scatterer is replaced by a set of surface currents  $\mathbf{e}$  and  $\mathbf{h}$  over the surface  $S$  so that in the exterior region the sources and fields are exactly the same as those existing in the original scattering problem, while they are zero in the interior region. The total electric field outside the scatterer  $\mathbf{E}(\mathbf{r})$  for  $\mathbf{r} \in \Omega_s$  is given by

$$\begin{aligned} \mathbf{E}(\mathbf{r}) = & \mathbf{E}_0(\mathbf{r}) + \nabla \times \int_S \mathbf{e}_i(\mathbf{r}') \cdot \mathbf{G}(k_S|\mathbf{r} - \mathbf{r}'|) dS \\ & - \nabla \times \nabla \times \int_S \frac{1}{jk\epsilon_S} \mathbf{h}_i(\mathbf{r}') \cdot \mathbf{G}(k_S|\mathbf{r} - \mathbf{r}'|) dS, \end{aligned} \quad (1)$$

$\mathbf{G}(k_S|\mathbf{r} - \mathbf{r}'|)$  is the Green's dyadic for the unbounded space,  $\mathbf{E}(\mathbf{r}) = 0$  for  $\mathbf{r} \in \Omega_i$ .

Now  $z_p$  denotes a rigid translation of the original coordinate system along the  $z$  axis with  $O_p$  as the origin of the new coordinate system. Then the total electric field in  $O_p$  is expanded in terms of spherical vector wavefunctions (SVWF) of the first kind  $M_{mn}^1(k_S r_p)$  and  $N_{mn}^1(k_S r_p)$ , i.e.

$$\begin{aligned} \mathbf{E}(\mathbf{r}_p + z_p \mathbf{e}_3) & = \sum_{m \in Z} \sum_{n \geq \max(1, |m|)} D_{mn} [a_{mn}^{(p)} (\mathbf{e}_i - \mathbf{e}_0, \mathbf{h}_i - \mathbf{h}_0) \\ & \quad \cdot M_{mn}^1(k_S r_p) + b_{mn}^{(p)} (\mathbf{e}_i - \mathbf{e}_0, \mathbf{h}_i - \mathbf{h}_0) \cdot N_{mn}^1(k_S r_p)], \end{aligned} \quad (2)$$

where  $D_{mn}$  is a normalization constant,  $\mathbf{e}_0 = \mathbf{n} \times \mathbf{E}_0$ ,  $\mathbf{h}_0 = \mathbf{n} \times \mathbf{H}_0$ ,

$$\begin{aligned} a_{mn}^{(p)} & = \frac{ik_S^2}{\pi} \int_S \left[ \mathbf{e} \cdot M_{mn}^{(2)}(k_S r'_p) + j \sqrt{\frac{\mu_S}{\epsilon_S}} \mathbf{h} \cdot N_{mn}^{(2)}(k_S r'_p) \right] dS, \\ b_{mn}^{(p)} & = \frac{ik_S^2}{\pi} \int_S \left[ \mathbf{e} \cdot N_{mn}^{(2)}(k_S r'_p) + j \sqrt{\frac{\mu_S}{\epsilon_S}} \mathbf{h} \cdot M_{mn}^{(2)}(k_S r'_p) \right] dS. \end{aligned} \quad (3)$$

Let the set  $\{z_p\}_{p=\overline{1, \infty}} = \Gamma_z$ , where  $\Gamma_z \subset \Omega_i$  is a segment of the  $z$ -axis. Then the system of the tangential components of the lowest-order SVWF with multiple origins is complete on  $S$ , and the infinite set of integral equations assures the nullfield condition for the total electric field within the enclosed volume [5]. The surface currents can be approximated by

$$\begin{aligned} \begin{pmatrix} \mathbf{e}_i^{\hat{N}} \\ \mathbf{h}_i^{\hat{N}} \end{pmatrix} & = \sum_{m=-M}^M \sum_{p=1}^N \\ & \times \alpha_{mp} \begin{pmatrix} \mathbf{n} \times M_{m,|m|+l}^1(k_i r'_p) \\ -j\sqrt{\epsilon_i/\mu_i} (\mathbf{n} \times N_{m,|m|+l}^1(k_i r'_p)) \end{pmatrix} \\ & + \beta_{mp} \begin{pmatrix} \mathbf{n} \times N_{m,|m|+l}^1(k_i r'_p) \\ -j\sqrt{\epsilon_i/\mu_i} (\mathbf{n} \times M_{m,|m|+l}^1(k_i r'_p)) \end{pmatrix}. \end{aligned} \quad (4)$$

This enables us to obtain the amplitude as a solution of the truncated system of integral equations

$$\begin{aligned} a_{m,|m|+l}^{(p)} (\mathbf{e}_i^{\hat{N}} - \mathbf{e}_0, \mathbf{h}_i^{\hat{N}} - \mathbf{h}_0) & = 0, \\ b_{m,|m|+l}^{(p)} (\mathbf{e}_i^{\hat{N}} - \mathbf{e}_0, \mathbf{h}_i^{\hat{N}} - \mathbf{h}_0) & = 0, \end{aligned} \quad (5)$$

$m = \overline{-M, M}$ ,  $p = \overline{1, N}$  with  $\hat{N}$  as a complex index incorporating  $M$  and  $N$ .

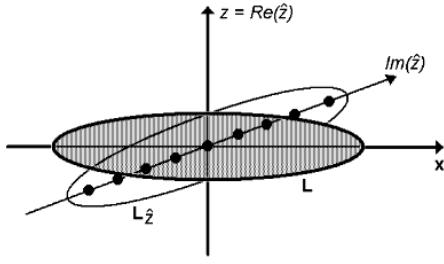


**Figure 1.** Sketch to demonstrate the concept of discrete sources on a complex plane.

If the sequences  $(e_i^{\hat{N}}, h_i^{\hat{N}})$  as solutions of the above scheme converge in the mean-square norm on  $S$  at  $(e_i, h_i)$ , then  $(e_i, h_i)$  represent the unique surface currents of the scattering problem. The approximate solution of the scattered field

$$\begin{aligned} \mathbf{E}_s^{\hat{N}}(\mathbf{r}) &= \nabla \times \int_S e_i^{\hat{N}} \cdot \mathbf{G}(k_s|\mathbf{r} - \mathbf{r}'|) dS \\ &\quad - \nabla \times \nabla \times \int_S \frac{1}{jk\epsilon_s} h_i^{\hat{N}} \cdot \mathbf{G}(k_s|\mathbf{r} - \mathbf{r}'|) dS, \quad \mathbf{r} \in \Omega_s \end{aligned} \quad (6)$$

concentrates on obtaining an approximate solution on the surface  $S$ . In a  $T$ -matrix scheme the scattered field outside a circumscribed sphere is expanded in terms of SVWF and the transition matrix, which relates the scattered field coefficients to the incident field coefficients, is computed. This is fully outlined in [5] and [30]. Once the internal surface currents are determined a formal solution of the scattered field can be constructed in the form (6). Energy characteristics in the far zone can be computed from the far field vector amplitude  $\mathbf{F}_s^{\hat{N}}(\theta, \varphi)$

$$\mathbf{F}_s^{\hat{N}}(\theta, \varphi) = \lim_{r \rightarrow \infty} \mathbf{E}_s^{\hat{N}}(\mathbf{r}) \cdot r e^{-jk_s r}. \quad (7)$$

The differential scattering cross section (DSCS) is calculated from

$$\sigma_d^{\hat{N}} = \left| \mathbf{F}_s^{\hat{N}} \right|^2. \quad (8)$$

Now we take an axially symmetrical scatterer with the  $z$ -axis as the symmetry axis of the particle. It is possible to reduce the problem of surface approximation to a sequence of one-dimensional problems relative to Fourier harmonics of the surface currents by using a system of multipoles distributed along the scatterer's axis of revolution and by expanding the external excitation in Fourier series. The approximation of the field on the surface  $S$  simplifies to the approximation of its Fourier harmonics on the generatrix  $L$  of the surface of revolution  $S$ . So multipoles situated on the axis of revolution adequately describe the particle geometry for prolate scatterers. But obviously this arrangement is not suitable for oblate scatterers. Therefore, as Eremin *et al* [31] suggested, we define a half-plane  $\varphi = \text{const}$ :  $\Phi = \{(\rho, z) | \rho \geq 0, z \in \Re\}$  with a complex plane  $\hat{\Phi} = \{\hat{z} = (\text{Re}(\hat{z}), \text{Im}(\hat{z})) | \text{Re}(\hat{z}), \text{Im}(\hat{z}) \in \Re\}$  in such a way that the real axis  $\text{Re}(\hat{z})$  coincides with the  $z$ -axis to situate the multipoles describing the scatterer. The spherical harmonics can be expressed in terms of the coordinates of the source point

$\hat{M}(\hat{z}) \in \hat{\Phi}$  and the observation point  $M(\rho, z) \in \Phi$  by using the analytic continuation procedure

$$\begin{aligned} M_{mn}^{1(3)}(k\mathbf{R}) &= z_n(kR) \left\{ im \frac{P_n^{|m|}(\cos \hat{\theta})}{\sin \hat{\theta}} [\sin(\theta - \hat{\theta}) \mathbf{i}_r \right. \\ &\quad \left. + \cos(\theta - \hat{\theta}) \mathbf{i}_\theta] - \frac{dP_n^{|m|}(\cos \hat{\theta})}{d\hat{\theta}} \mathbf{i}_\varphi \right\} e^{im\varphi} \\ N_{mn}^{1(3)}(k\mathbf{R}) &= \left\{ n(n+1) \frac{z_n(kR)}{kR} P_n^{|m|} \right. \\ &\quad \times (\cos \hat{\theta}) [\cos(\theta - \hat{\theta}) \mathbf{i}_r - \sin(\theta - \hat{\theta}) \mathbf{i}_\theta] \\ &\quad \left. + \frac{[kR \cdot z_n(kR)]'}{kR} \frac{dP_n^{|m|}(\cos \hat{\theta})}{d\hat{\theta}} \right. \\ &\quad \times [\sin(\theta - \hat{\theta}) \mathbf{i}_r + \cos(\theta - \hat{\theta}) \mathbf{i}_\theta] \\ &\quad \left. + \frac{[kR \cdot z_n(kR)]'}{kR} \cdot im \frac{P_n^{|m|}(\cos \hat{\theta})}{\sin \hat{\theta}} \mathbf{i}_\varphi \right\} e^{im\varphi} \end{aligned} \quad (9)$$

where  $z_n(kR)$  stays for the spherical Bessel functions  $j_n(kR)$  or the spherical Hankel functions  $h_n^1(kR)$ ,  $(\mathbf{i}_r, \mathbf{i}_\theta, \mathbf{i}_\varphi)$  are the unit vectors in spherical coordinates,  $R^2 = \rho^2 + (z - \hat{z})^2$ ,  $\sin \hat{\theta} = \rho/R$ ,  $\cos \hat{\theta} = (z - \hat{z})/R$  and  $R$  is taken to be a branch corresponding to an arithmetical root on the real axis  $z$ . Figure 1 shows how the boundary  $L_{\hat{z}}$  of the domain  $D_{\hat{z}} \in \hat{\Phi}$  coincides with the image of the curve  $L$ . The point  $\hat{M}(\hat{z}) \in \hat{\Phi}$  is called the image of the point  $M(\rho, z) \in \Phi$  if  $R_{M\hat{M}}^2 = \rho^2 + (z - \hat{z})^2 = 0$  [31]. An approximate solution for the surface currents can be constructed in the form of (4), (5) if a set of discrete poles  $\{\hat{z}_p\}_{p=1, \infty} \subset D_{\hat{z}}$  have at least one limit point in  $D_{\hat{z}}$ , i.e.  $\hat{z}_0 = \lim_{p \rightarrow \infty} \hat{z}_p$ ,  $\hat{z}_0 \in D_{\hat{z}}$ .

### 3. Discrete source method

As the DSM is used as a reference we will give a short description of the theory in the following.

The DSM is a well known semi-analytical method which has recently been extended to oblate scatterers. In the frame of DSM the approximate solution of the boundary value problem is constructed as a finite linear combination of the field of dipoles and multipoles deposited in some supplementary domain. Under these conditions the representation of the approximate solution satisfies Maxwell equations in  $\Omega_{i,s}$  and the Silver–Müller radiation condition at infinity. The unknown amplitudes of discrete sources (DSs) are to be determined from the transmission conditions at the boundary  $S$ . So, the boundary value scattering problem under investigation is reduced to the solution of an approximation problem enforced at an obstacle surface [32]. Besides, the DSM allows us to make sufficient use of the axial symmetry of a scatterer, reducing the three-dimensional surface approximation problem to a number of one-dimensional problems, that appreciably shortens the calculating time.

Another attractive feature of the DSM consists in the flexible choice of DS fields that can be used for approximate solution construction. Additionally, there are no limitations to a choice of support of DS, which should provide fulfilling Maxwell equations, radiation conditions and yield a complete system of DS fields at the obstacle surface [32]. For the oblate

obstacles it is not possible to deposit the supplementary domain inside the scatterer. One of the possibilities the DSM gives is to deposit the DS in a complex plane similar to the previous section. Such a procedure allows us to limit the DS sequence when  $N \rightarrow \infty$ . The limitation is very important to provide the stability of the numerical model based on the DSM. The procedure of construction of the analytic continuation of DS support to the complex plane is discussed by Eremina *et al* [15].

We will construct the approximate solution by taking into account not only the rotational symmetry of the obstacle, but also the polarization of an external excitation as well. We will consider the case of parallel polarization of the plane wave; the case of a perpendicular polarized plane wave can be found in the paper of Eremina *et al* [15]. Then the external excitation accepts the following form:

$$\mathbf{E}^0 = (e_x \cos \theta_0 + e_z \sin \theta_0) \gamma,$$

$$\mathbf{H}^0 = -e_y \gamma \cos \theta_0,$$

$$\gamma = \exp \{-jk_s (x \sin \theta_0 - z \cos \theta_0)\}.$$

To take into account the polarization of the external excitation we use some linear combination of electrical and magnetic multipoles. For this we need special vector potentials. The representation for vector potentials in a cylindrical coordinate system can be presented as

$$\begin{aligned} \mathbf{A}_{mn}^{1,s,i} &= \{Y_m^{e,i}(\eta, w_n^{s,i}) \cos(m+1)\phi; \\ &\quad -Y_m^{s,i}(\eta, w_n^{s,i}) \sin(m+1)\phi; 0\}, \\ \mathbf{A}_{mn}^{2,s,i} &= \{Y_m^{e,i}(\eta, w_n^{s,i}) \sin(m+1)\phi; \\ &\quad Y_m^{s,i}(\eta, w_n^{s,i}) \cos(m+1)\phi; 0\}. \end{aligned} \quad (10)$$

Vector potentials for vertical dipoles, which are required to provide completeness of the multipoles' system, are

$$\mathbf{A}_n^{3,s,i} = \{0, 0, Y_0^{s,i}(\eta, w_n^{s,i})\}, \quad (11)$$

where

$$Y_m^{e,i}(\eta, w_n^{e,i}) = j_m \left( k_{e,i} R_{\eta \omega_n^{e,i}} \right) \left( \frac{r}{R_{\eta \omega_n^{e,i}}} \right). \quad (12)$$

So, the approximate solution taking into account P-polarization of the plane wave, axial symmetry of the particle, can be represented in the form

$$\begin{aligned} \begin{pmatrix} \mathbf{E}_{s,i}^N \\ \mathbf{H}_{s,i}^N \end{pmatrix} &= \sum_{m=0}^M \sum_{n=1}^{N_{s,i}^m} \{p_{mn}^{s,i} D_1 \mathbf{A}_{mn}^{1,s,i} + q_{mn}^{s,i} D_2 \mathbf{A}_{mn}^{2,s,i}\} \\ &\quad + \sum_{n=1}^{N_{s,i}^0} r_n^{s,i} D_1 \mathbf{A}_n^{1,s,i} \end{aligned} \quad (13)$$

where

$$D_1 = \begin{pmatrix} \frac{j}{k \epsilon_{s,i} \mu_{s,i}} \nabla \times \nabla \\ -\frac{j}{\mu_{s,i}} \nabla \end{pmatrix}, \quad D_2 = \begin{pmatrix} \frac{1}{\epsilon_{s,i}} \nabla \\ \frac{j}{k \epsilon_{s,i} \mu_{s,i}} \nabla \times \nabla \end{pmatrix}.$$

Then the following result holds.

The approximate solution (13) converges to the exact one as  $\{M, N_{s,i}^m\}$  tend to infinity [5].

The approximate solution (13) satisfies Maxwell's equation and radiating conditions and can be presented as a finite linear combination of Fourier harmonics with respect to the  $\phi$  angle variable. So, at first we resolve the plane wave excitation into a Fourier series with respect to the  $\phi$  variable, using the following resolution for the plane wave:

$$\begin{aligned} &\exp \{-jk_s \rho \sin \theta_0 \cos \phi\} \\ &= \sum_{m=0}^{\infty} (2 - \delta_{0m}) (-j)^m J_m(k_s \rho \sin \theta_0) \cos m\phi, \end{aligned} \quad (14)$$

where  $\theta_1$  is the incident angle of the plane wave.

The approximate solution satisfies all the conditions of the original scattering problem, except the transmission conditions. Therefore, the unknown vector of amplitudes of DS

$$\mathbf{p}_m = \{p_{mn}^{s,i}, q_{mn}^{s,i}, r_n^{s,i}\}_{n=1}^{N_{s,i}^m} \quad (15)$$

where  $p_{mn}^{s,i}$  are amplitudes of electric,  $q_{mn}^{s,i}$  magnetic and  $r_n^{s,i}$  vector dipoles in the representation (13), is to be determined from the transmission conditions on the particle surface. Taking into account the dependence of the plane wave on the  $\varphi$  angle, we can reduce the surface approximation problem enforced at the particle surface to a sequence of one-dimensional problems at the particle generatrix  $L$ . To solve this problem the general matching-point technique is used. At first we choose matching points  $\{\eta_l\}_{l=1}^L$  distributed homogeneously over  $L$ . Then by matching the representation for the approximate solution and external excitation at the set of matching points and using the axial symmetry we pass from the surface approximation to the approximation for each Fourier harmonic. As a consequence the unknown vectors of amplitudes  $\mathbf{p}_m$  can be found as a pseudosolution of a over-determined system of linear equations [5].

The main feature of the extended DSM algorithm described above compared to the conventional DSM one [32] consists in the deposition of DS in a complex plane.

After the DS amplitudes  $\{\mathbf{p}_m\}_{m=-1}^M$  have been determined, the far field pattern can be computed:

$$\frac{\mathbf{E}(\mathbf{r})}{|\mathbf{E}^0(\mathbf{r})|} = \frac{\exp(-jk_s r)}{r} \mathbf{F}(\theta, \phi) + o\left(\frac{1}{r}\right), \quad r \rightarrow \infty. \quad (16)$$

The vector  $\mathbf{F}(\theta, \phi)$  has two components in the far zone  $\phi$  and  $\theta$ , so that its components are determined at the unit sphere as

$$\mathbf{F}(\theta, \phi) = \theta \cdot F_\theta(\theta, \phi) + \phi \cdot F_\phi(\theta, \phi). \quad (17)$$

Using an asymptotic representation for  $Y_{mn}$  the components for parallel and perpendicular polarizations can be calculated analytically [15].

#### 4. Cassini ovals

To simulate light scattering by small, concave particles it is necessary to find an appropriate mathematical description of the particle shape. This can be done easily by the usage of Cassini curves. For example, this approach is used to fit the shape of the human red blood cell [12–14].

In 1680 Giovanni Domenico Cassini (1625–1712), also known as Jean-Dominique Cassini, introduced a term to describe a special group of curves. These curves are

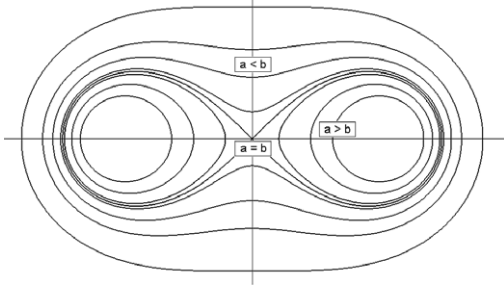


**Figure 2.** Cassini ovals for a given  $a$  and varying values of  $b$ .

characterized in such a way that the product of the distance of two fixed focal points is constant (while for a normal ellipse the sum of the distance of two fixed focal points is constant).

The Cassini ovals have the Cartesian equation

$$[(x - a)^2 + y^2][(x + a)^2 + y^2] = b^4. \quad (18)$$

This leads to

$$y = \pm \left( -a^2 - x^2 \pm (4x^2a^2 + b^4)^{\frac{1}{2}} \right)^{\frac{1}{2}}. \quad (19)$$

There is also a polar notation:

$$r^4 + a^4 - 2a^2r^2 \cos(2\theta) = b^4, \quad (20)$$

which means for  $r$

$$r = \pm \left( a^2 \left[ \cos(2\theta) \pm \left( \frac{b^4}{a^4} - \sin^2(2\theta) \right)^{\frac{1}{2}} \right] \right)^{\frac{1}{2}}. \quad (21)$$

Note that this is not the same result for  $r$  one gets by transforming (18) into polar coordinates by substituting  $x = r \cos(\theta)$  and  $y = r \sin(\theta)$ . The expression in polar coordinates corresponding to (18) is

$$r = \left( a^2 - 2a^2 \sin^2(\theta) + (-4a^4 \sin^4(\theta)^2 + 4a^4 \sin^2(\theta) + b^4)^{\frac{1}{2}} \right)^{\frac{1}{2}}. \quad (22)$$

The Cassini shape therefore depends on the relation  $b/a$ . If  $a < b$  the curve is an oval loop, for  $a = b$  the result is a lemniscate (like the  $\infty$ -symbol) and for  $a > b$  the curve consists of two separate loops. Figure 2 gives an overview of some of the resulting curves.

If  $a$  is chosen slightly smaller than  $b$  one gets a concave, bone-like shape. This concavity will get deeper the closer  $a$  gets to  $b$ . By rotating this two-dimensional curve around the vertical axis we get a three-dimensional particle in the shape of an oblate discsphere with a concavity on its top and bottom sides; see figure 3.

The variation of  $a$  and  $b$  allows us to create different shapes so that the diameter, thickness and form of the concavity can be influenced. Unfortunately, this influence is an indirect one because  $a$  and  $b$  are not related directly to diameter or thickness; changing the value of one of these parameters changes both characteristics.

By adding a factor  $c$  in front of (19)

$$y = c \left( -a^2 - x^2 + (4x^2a^2 + b^4)^{\frac{1}{2}} \right)^{\frac{1}{2}}. \quad (23)$$

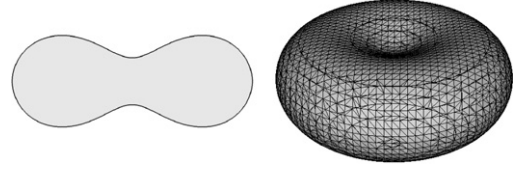


**Figure 3.** Example for an oblate discsphere with concavity gained by Cassini curves. Left, two-dimensional profile; right, three-dimensional particle shape for parameters  $a = 5$  and  $b = 5.2$ . The three-dimensional shape is shown with a grid model to give a better impression of the shape; the grid is not needed for light scattering simulation.

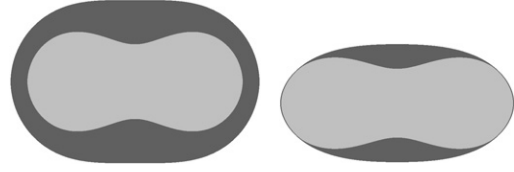


**Figure 4.** Influence of parameters on particle size. Left:  $a = 0.5$ ,  $b = 0.55$  (inner concave shape) and  $a = 0.5$ ,  $b = 0.7$  (outer convex shape) respectively;  $c = 1.2$  in both cases. Diameter and thickness of the Cassini-shaped particle increases the greater  $b$  gets. Right:  $a = 0.5$ ,  $b = 0.55$ ,  $c = 1.0$  (inner concave shape) and  $a = 0.4$ ,  $b = 0.63$ ,  $c = 0.8$  (outer convex shape). In this case both shapes have nearly the same diameter and the outer curves have the same radius.

one gets a better flexibility for changing the shape as it enables us to regulate the thickness directly.

Equation (23) will be used to describe all the following particles for which light scattering is calculated in this paper.

## 5. Results

In this section we would like to present light scattering NFM-DS results for different particle shapes and to compare them to the DSM results.

For the first shape we choose  $a = 0.5$  and  $b = 0.7$  and inflate it by  $c = 1.2$  to keep the aspect ratio—the relation between diameter and thickness—low. Then we decrease the values of  $b$  in 0.05 steps down to 0.55. This leads to particles with diameters between 1.49 and 1.72  $\mu\text{m}$ ; the corresponding aspect ratios are between 1.47:1 and 2.05:1. The resulting shapes are given alongside the scattering diagrams for an incident wavelength of 632.8 nm and a refractive index of 1.46, which are presented in figure 5.

One can see that there is a perfect congruence between both methods.

As this, in general, demonstrates that the NFM-DS is capable of calculating light scattering by nonspherical shapes with concavities we now would like to investigate the influence of these concavities on the scattering pattern further. For this it is reasonable to keep the diameter and the outer curve of the particle constant; only the area around the vertical axis should be varied from concave to convex. So the results from figure 5 are not suitable for this. As stated above changing the Cassini parameters  $a$  and  $b$  influence diameter and thickness and this cannot be controlled directly. For constant values of  $a$  and decreasing values of  $b$  diameter and thickness also decrease. This can be observed from the shapes presented in figure 5;

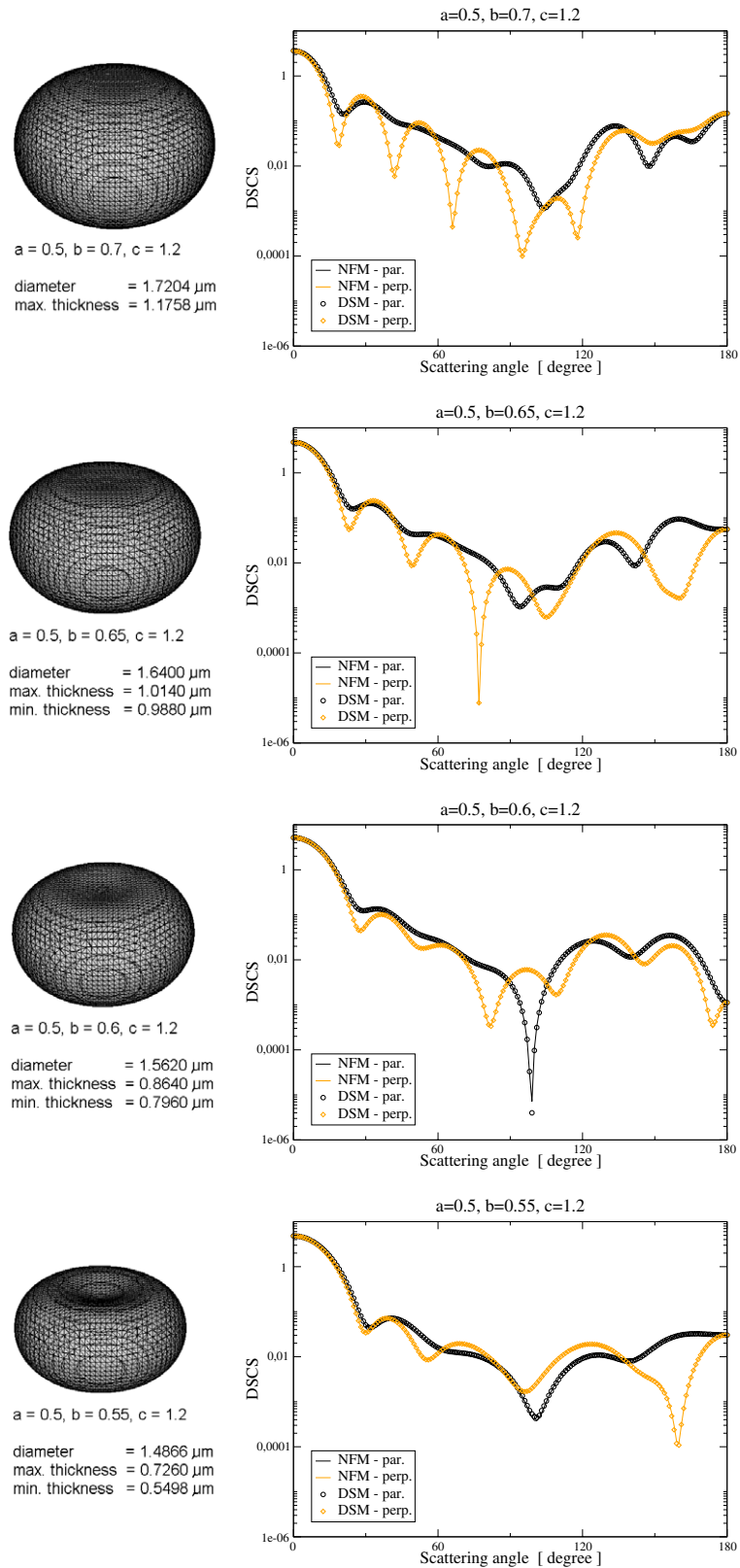


**Figure 5.** Light scattering results for Cassini-shaped particles; comparison between NFM-DS and DSM. Shown are the results for parallel and perpendicular DSCS. Wavelength is  $\lambda = 632.8 \text{ nm}$ , refraction index is 1.46. The direction of incident light is parallel to the rotational axis. Note that the first shape (top) is convex while the others are concave.

additionally, the values for diameter and main thickness are specified. To make this effect more obvious, figure 4 (left)

shows the profiles for the used shapes with  $b = 0.55$  and  $0.7$  respectively.

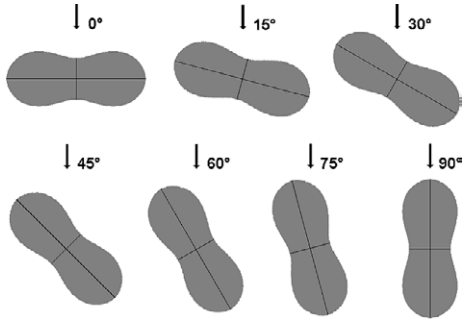


**Figure 6.** Sketch to demonstrate the position of the concave Cassini-shaped particle regarding the incident light.

To investigate the influence of the concavities we need other Cassini shapes with different parameters. We want both shapes to have the same diameter and a similar gradient of shape in the outer area. For this we choose one concave shape with  $a = 0.5$ ,  $b = 0.55$  and  $c = 1.0$ , which is in principle the same concave shape we used before but with a higher aspect ratio. The diameter is  $1.49 \mu\text{m}$ , the aspect ratio is 2.46:1. Now we need a corresponding convex shape, which can be created by choosing  $a = 0.4$ ,  $b = 0.63$  and  $c = 0.8$ . Diameter and outer curves are quite similar; the aspect ratio is 1.92:1. This is presented in figure 4 (right).

For these two particle shapes not only light scattering for incident light parallel to the symmetry-axis, but also for

different angles  $\theta$  between the axis of symmetry and the incident light is calculated now. For  $\theta$  a range between  $\theta = 0^\circ$  and  $90^\circ$ , divided into  $15^\circ$  steps, is chosen, the wavelength is  $632.8 \text{ nm}$  and the refractive index is 1.46. Figure 6 gives an impression about the position of the particle shape regarding the incident light.

This calculation of light scattering under different incident angles can be done with low computational efforts as the  $T$ -matrix is already computed. To check whether we get reasonable results we first compare the NFM-DS results with those we get from the DSM for the concave shaped particle shown in figure 4 (right). Figure 7 shows the scattering diagrams for  $\theta = 0^\circ, 30^\circ, 60^\circ$  and  $90^\circ$ . Again we get perfect congruence between both methods.

In the next step we compare the scattering patterns for the concave particle to the convex one (figure 4—right). The results are presented in figure 8. As we calculate the far field pattern, the main peak can be found at the forward scattering area. This peak changes its position in the scattering diagram according to the angle  $\theta$  of the incident light. At this ‘shadow’ side the influence of the concavity is not so obvious as at the area of back-scattering. There one can observe the main influence of the concavity on the scattering pattern in that range, where it has its maximum. This divergence becomes smaller at the outer area of the particle where the concavity gets less distinct. The area of divergence also changes its position according to  $\theta$ . Additionally the effect of the concavity decreases in general for higher values of  $\theta$  as its effective size gets lower for increasing values of  $\theta$ . So for  $\theta = 90^\circ$

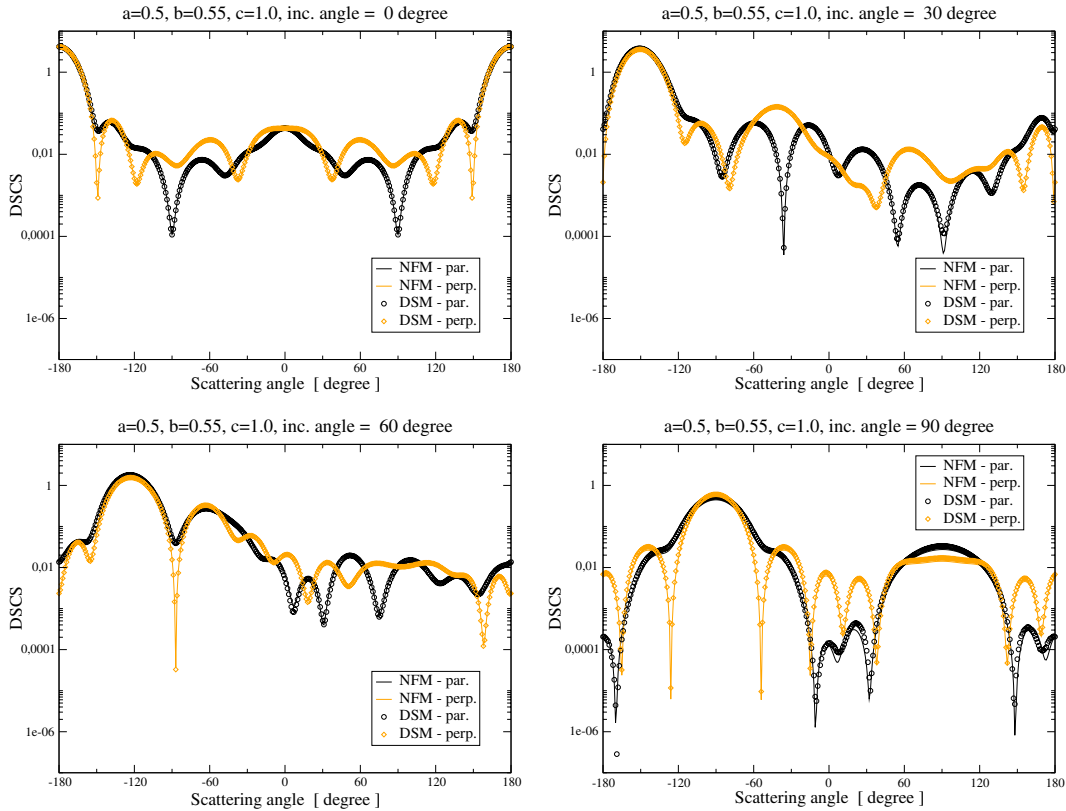


**Figure 7.** Light scattering results for a concave Cassini-shaped particle; comparison between NFM-DS and DSM. The angle  $\theta$  between the direction of incident light and rotational axis is varying from  $0^\circ$  to  $90^\circ$  in  $30^\circ$  steps. The results for parallel and perpendicular DSCS are shown. Wavelength is  $\lambda = 632.8 \text{ nm}$ , refractive index is 1.46.

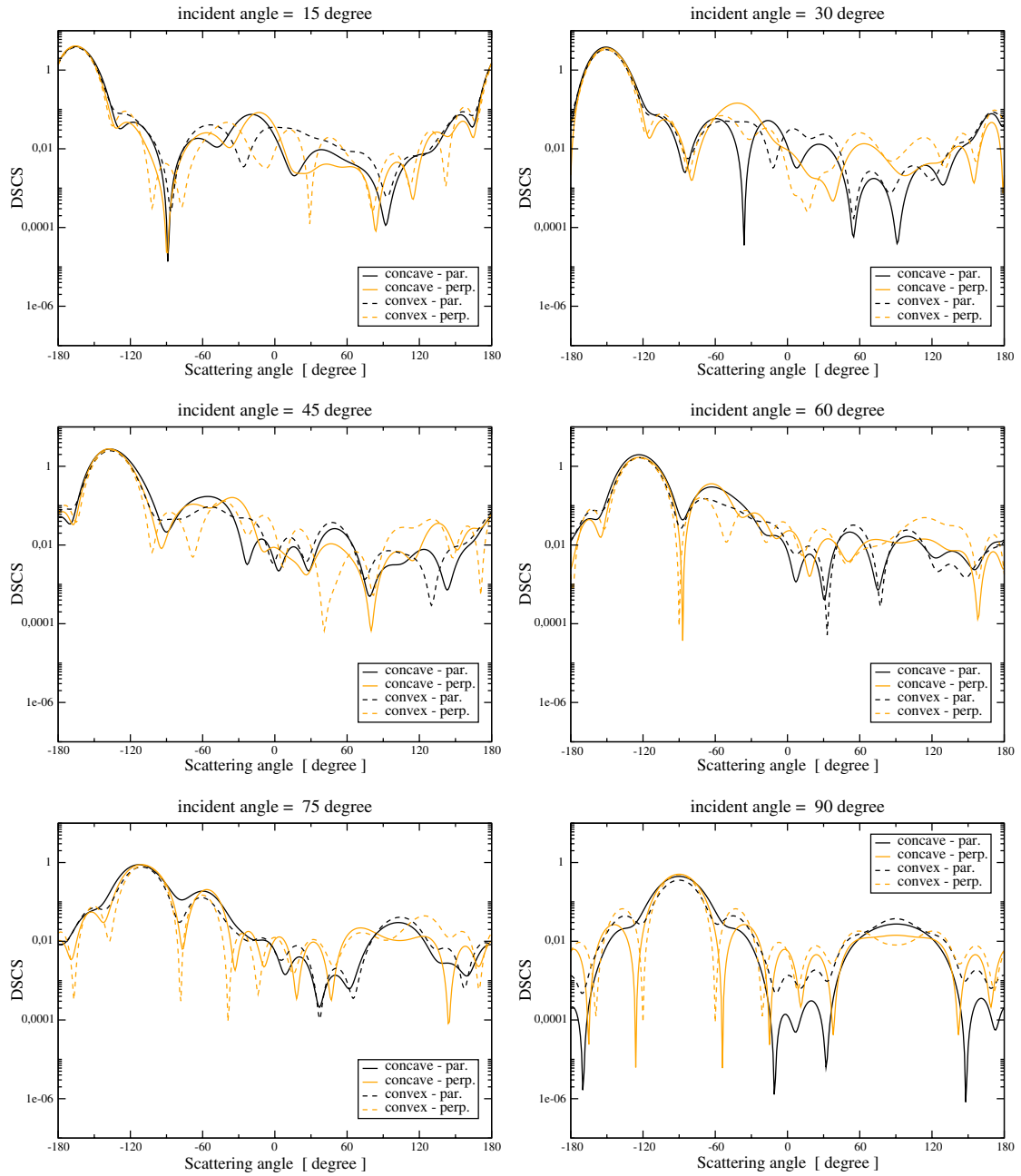


**Figure 8.** Light scattering results gained by NFM-DS for a concave Cassini-shaped particle compared to a convex one. The angle  $\theta$  between the direction of incident light and rotational axis is varying from 15° to 90° in 30° steps. The results for parallel and perpendicular DSCS are shown. Wavelength is  $\lambda = 632.8$  nm, refraction index is 1.46.

the influence of the concavity nearly vanishes and is overlaid by the effects caused by the bigger volume of the convex shape.

## 6. Summary and conclusion

The NFM-DS is applied to calculate light scattering by concave particles. As input data shape nonspherical biconcave Cassini ovals are used. This description of particle shapes allows us to get different kinds of shapes—concave as well as convex—just by changing three parameters, and can be easily implemented into computer algorithms.

The comparison of the NFM-DS light scattering results to those we get from DSM shows good congruence.

Additionally, light scattering for different incident angles of the incoming light is calculated. These results also coincide with those from DSM and the curves in the scattering diagrams show the expected gradients.

By this it is demonstrated that the NFM-DS is capable of calculating light scattering by nonspherical particles with concavities. This is a big advancement as it expands the range of light scattering problems which can be solved by  $T$ -matrix methods. We hope that with this approach it will be possible to simulate light scattering by the real shape erythrocyte [33].

## Acknowledgment

We would like to acknowledge support of this work by Deutsche Forschungsgemeinschaft (DFG).

## References

- [1] Wriedt T 1998 *Part. Part. Syst. Charact.* **15** 67–74
- [2] Kahnert F M 2003 *J. Quantum Spectrosc. Radiat. Transfer* **79/80** 775–824
- [3] Waterman P C 1965 *Proc. IEEE* **53** 805–12
- [4] Mishchenko M I, Travis L D and Mackowski D W 1996 *J. Quantum Spectrosc. Radiat. Transfer* **55** 535–75
- [5] Doicu A, Eremin Y and Wriedt T 2000 *Acoustic and Electromagnetic Scattering Analysis using Discrete Sources* (San Diego, CA: Academic)
- [6] Nilsson A M K, Alsholm P, Karlsson A and Andersson-Engels S 1998 *Appl. Opt.* **37** 2735–48
- [7] Karlsson A, He J P, Swartling J and Andersson-Engels S 2005 *IEEE Trans. Biomed. Eng.* **52** (1)
- [8] Mazon P, Muller S and El Azouzi H 1997 *Eur. Biophys. J.* **26** 247–52
- [9] Wysoczanski D, Mroczka J and Onofri F 2002 *11th Int. Symp. on Applications of Laser Techniques to Fluid Mechanics (Lisboa, Portugal)*
- [10] Farafonov V G and Il'in V B 1992 *Meas. Sci. Technol.* **13** 331–5
- [11] Green K, Lumme K and Penttila A 2001 *DPS 33rd Mtg (New Orleans, USA)*
- [12] Angelov B and Mladenov I M 1999 *Geometry, Integrability and Quantization* ed I Mladenov and G Naber (Sofia: Coral Press) pp 27–47
- [13] Mazon P and Muller S 1998 *J. Opt.* **29** 68–77
- [14] Di Biasio A and Cametti C 2005 *Bioelectrochemistry* **65** 163–9
- [15] Eremina E, Eremin Y and Wriedt T 2005 *Opt. Commun.* **244** 15–23
- [16] Wriedt T (ed) 1999 *Mechanics and Mathematical Methods vol 4 Generalized Multipole Techniques for Electromagnetic and Light Scattering* (Amsterdam: Elsevier)
- [17] Wriedt T, Eremina E and Schuh R 2005 *8th Conf. on Electromagnetic and Light Scattering by Nonspherical Particles: Theory, Measurements and Applications (Salobrena, Granada, Spain)*
- [18] Waterman P C 1969 *J. Acoust. Soc. Am.* **45** 1417–29
- [19] Waterman P C 1971 *Phys. Rev. D* **3** 825–39
- [20] Bostrom A 1984 *J. Acoust. Soc. Am.* **76** 588–93
- [21] Bates R H T and Wall D J N 1977 *Phil. Trans. R. Soc. A* **287** 45–117
- [22] Hackman R H 1984 *J. Acoust. Soc. Am.* **75** 35–45
- [23] Doicu A and Wriedt T 1997 *Opt. Commun.* **139** 85–98
- [24] Wriedt T and Doicu A 1998 *J. Mod. Opt.* **45** 199–214
- [25] Pulbere S and Wriedt T 2004 *Part. Part. Syst. Charact.* **21** 213–8
- [26] Hellmers J, Wriedt T and Doicu A 2005 *J. Mod. Opt.* at press
- [27] Wiscombe W J and Mugnai A 1985 *NASA Reference Publication* **1157** 1–277
- [28] Mishchenko M I, Travis L D and Lacis A A 2002 *Scattering, Absorption and Emission of Light by Small Particles* (Cambridge: Cambridge University Press)
- [29] Wauer J, Schmidt K, Rother T, Ernst T and Hess M 2004 *Appl. Opt.* **43** 6371–9
- [30] Doicu A and Wriedt T 1999 *J. Opt. Soc. Am. A* **16** 2539–44
- [31] Eremin Y A, Orlov N V and Rozenberg V I 1994 *Comput. Phys. Commun.* **79** 201–14
- [32] Eremin Y, Orlov N and Sveshnikov A 1999 *Generalized Multipole Techniques for Electromagnetic and Light Scattering* ed T Wriedt (Amsterdam: Elsevier Science) pp 39–80
- [33] Maltsev V P and Semyanov K A 2004 *Characterisation of Bio-Particles from Light Scattering* (Utrecht: VSP)